Thermal-wave detection and thin-film thickness measurements with laser beam deflection

Jon Opsal, Allan Rosencwaig, and David L. Willenborg

A new technique has been developed that employs highly focused laser beams for both generating and detecting thermal waves in the megahertz frequency regime. This technique includes a comprehensive 3-D depth-profiling theoretical model; it has been used to measure the thickness of both transparent and opaque thin films with high spatial resolution. Thickness sensitivities of ±2% over the 500–25,000-Å range have been obtained for Al and SiO_2 films on Si substrates.

I. Introduction

Thermal-wave physics is playing an ever-increasing role in the study of material parameters. It has been employed in optical investigations of solids, liquids, and gases with photoacoustic[1] and thermal lens[2] spectroscopy. Thermal waves have also been used to study the thermal and thermodynamic properties[1,3] of materials and for imaging thermal and material features within a solid sample.[4]

Thermal waves are present whenever there is periodic heat generation and heat flow in a medium. There are, therefore, a multitude of mechanisms by which these waves can be produced, with the two most common involving the absorption by the sample of energy from either an intensity-modulated optical beam[1] or from an intensity-modulated electron beam.[4] Several mechanisms are also available for detecting, directly or indirectly, the resulting thermal waves. These include gas-microphone photoacoustic detection of heat flow from the sample to the surrounding gas in which pressure changes are monitored[1,5]; photothermal measurements of infrared radiation emitted from the heated sample surface[6–8]; optical beam deflection of a laser beam traversing the periodically heated gaseous or liquid layer just above the sample surface[9–11]; interferometric detection of the thermoelastic displacements of the surface[12–14]; optical detection of the thermoelastic deformations of the surface[13–16]; and piezoelectric detection of thermoacoustic signals generated in the sample.[1,17,18]

To date, only this last technique involving thermoacoustic detection has been used routinely for detecting high-frequency (i.e., megahertz regime) thermal waves. The thermoacoustic detection methodology has, therefore, found important applications in thermal-wave imaging[4,19–21] at high spatial resolution, where micron-sized thermal waves are needed, as in the study of semiconductor materials and devices.

The use of a thermoacoustic probe to detect the reflection and scattering of the thermal waves from the thermal features suffers, however, from the major drawback of requiring acoustic coupling between the sample and an ultrasonic transducer. In the analysis of semiconductor materials and devices, one would like to operate in an open environment, employ completely contactless methods for thermal-wave generation and detection, and be able to make measurements or obtain images at high spatial resolution. This last requirement necessitates the use of a highly focused beam for thermal-wave generation and the capability for detecting high-frequency (>100-kHz) thermal waves.

To satisfy all the above conditions one needs to utilize lasers for both generating and detecting the thermal waves. The generation is, of course, straightforward. The detection is more involved, performed either by interferometric detection of the thermoelastic displacements of the sample surface or by laser detection of the local thermoelastic deformations of the surface. Both techniques are analogous to the optical methods used for detecting surface acoustic waves,[22,23] although here the surface displacements and deformations are due to the thermal waves. All the other methods for thermal-wave detection suffer from either being limited to low modulation frequencies or from needing contact to the sample.

There have been some initial studies of thermal-wave detection using the techniques described above. Ameri *et al.*[12] performed a rudimentary imaging experiment

The authors are with Therma-Wave, Inc., 47734 Westinghouse Drive, Fremont, California 94539.

Received 2 April 1983.
0003-6935/83/203169-08$01.00/0.

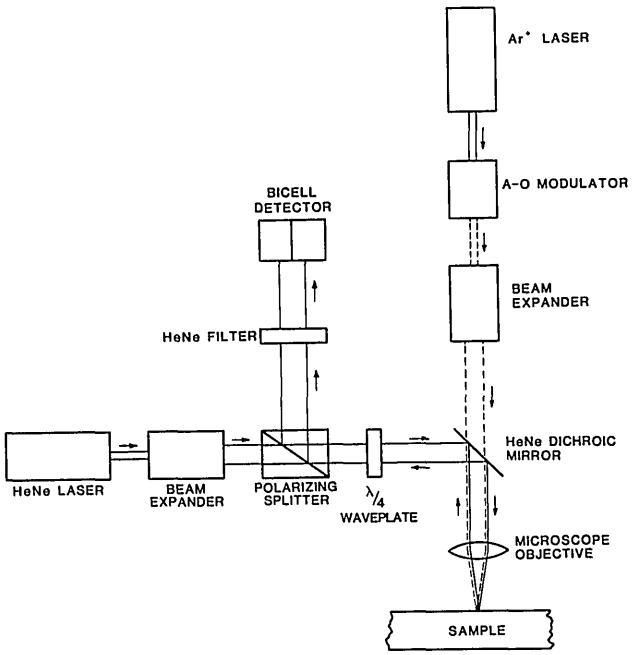

Fig. 1. Schematic depiction of laser beam deflection technique used for the thin-film thickness measurement experiments.

with the laser interferometric technique, while Amer and his colleagues[13–15] have both the laser interferometric and a laser deflection (surface deformation) technique for spectroscopic studies on amorphous silicon. These various investigations were all performed at low to moderate modulation frequencies (<100 kHz) only.

We have developed a laser beam deflection technique which, although similar to the method employed by Amer's group, differs in several important respects. In particular, our method employs highly focused heating and probe laser beams, both incident normal to the sample surface, and the experiments are performed at high modulation frequencies of up to 10 MHz.

Figure 1 depicts the experimental arrangement that we use. The 488-nm beam of a 100-mW Ar^+ ion laser is intensity-modulated with an acoustooptic modulator, directed through a beam expander, and then focused to a 2–4-μm diam spot on the sample. This is the heating beam, and it has a sample incident power of ~30 mW. The 633-nm beam of a 5-mW He–Ne laser, the probe beam, is directed through a beam expander, a polarizing beam splitter and quarterwave plate, reflected off a dichroic mirror, and then focused onto a 2–4-μm diam spot on the sample with an incident power of ~2 mW. The two laser spots are displaced ~2 μm from each other at the sample surface. The 488-nm heating beam reflects back on itself, while the 633-nm probe beam undergoes a periodic change in the local slope of the sample surface. The reflected probe beam passes through the quarterwave plate again, and since it is 90° out of phase from the beam leaving the He–Ne laser, it is directed by the polarizing beam splitter to the bicell photodetector, which measures the periodic deflections of the probe beam. Unlike the laser interferometric technique, which measures local surface displacements in the vertical direction, the laser probe method measures changes in the local slope of the surface as depicted in Fig. 2.

With the apparatus depicted in Fig. 1, we are able to detect, at a 1-MHz modulation frequency, changes in the local surface slope in Al that result from local surface displacements of $\sim 10^{-4}$ Å/$\sqrt{\text{Hz}}$, a sensitivity that is considerably greater than that reported in the recent experiments performed at much lower modulation frequencies with laser interferometric[12,14,15] and with laser probe deflection[13–15] methods.

In Sec. II we present the theory that, when combined with our thermal-wave measurement technique, gives us a system for performing quantitative thickness analyses of one or more films on a substrate. The theory we use is essentially the recent 1-D multilayer model of Opsal and Rosencwaig[24] (O-R model) extended appropriately to three dimensions.

In Sec. III we present some of our results showing good agreement between theory and experiment and, just as important, the sensitivity of our measurements to thickness variations. Finally, in Sec. IV we conclude with a brief summary.

II. Theory

A. Surface Temperatures

When a laser beam, intensity-modulated at a frequency ω, is focused onto a spot of radius a on the surface of a sample, the surface temperature at distance r from the beam center can be written as

$$T(r) = T_0 + T_1(r) + T_2(r)\cos(\omega t + \phi), \quad (1)$$

where T_0 is the ambient temperature, $T_1(r)$ is the

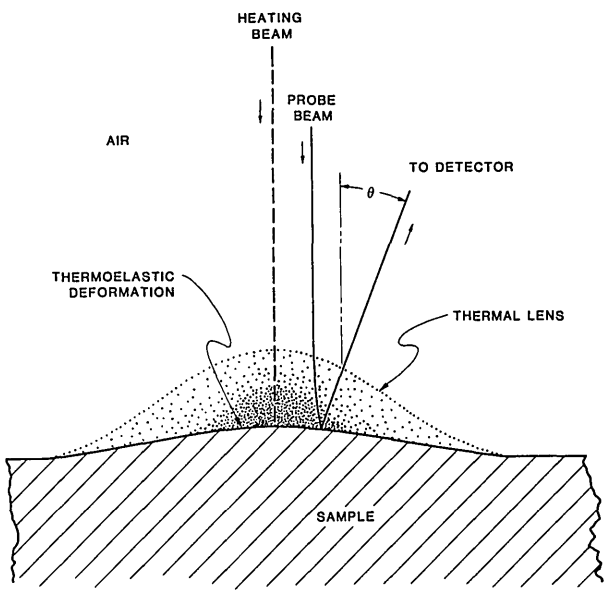

Fig. 2. Schematic depiction of physical processes affecting the laser probe beam for an opaque homogeneous sample including thermoelastic deformation of the air–sample interface and thermal lens effects in the air above the sample.

steady-state dc temperature, and $T_2(r)$ is the magnitude of the ac or oscillating temperature, which in general will have a nonzero phase ϕ. For a homogeneous sample (i.e., infinite half-space), 3-D analyses similar to those of Aamodt and Murphy[25] and McDonald[26] provide expressions for $T_1(r)$ and $T_2(r)$:

$$T_1(r) = \frac{P_0}{2\pi\kappa}\int dq\, \exp(-q^2a^2/4)J_0(qr), \tag{2a}$$

$$T_2(r) = \frac{P_0\mu}{2\pi\kappa}\left|\int qdq\, \frac{\exp(-q^2a^2/4)J_0(qr)}{\sqrt{q^2\mu^2 - 2i}}\right|, \tag{2b}$$

where P_0 is the power of a Gaussian probe beam of radius a, which is assumed to be absorbed at the surface. Also, in these expressions μ is the thermal diffusion length; $\mu = \sqrt{2\kappa/\omega\rho C}$, where κ is the thermal conductivity, ρ is the density, and C is the specific heat. J_0 is the cylindrical Bessel function of order zero.

At the center of the heating beam $r = 0$ we have

$$\frac{T_1(0)}{P_0} = \frac{1}{2\sqrt{\pi}\kappa a}, \tag{3a}$$

$$\frac{T_2(0)}{T_1(0)} = \frac{a}{\mu\sqrt{\pi}}\left|\int xdx\, \frac{\exp(-a^2x^2/4\mu^2)}{\sqrt{x^2 - 2i}}\right|, \tag{3b}$$

which are universal functions of κa and a/μ, respectively. The first of these, Eq. (3a), is plotted in Fig. 3(a) along with points for a number of different materials assuming a beam radius $a = 1$ μm. For a good thermal conductor such as aluminum we expect a temperature rise of ~1°C for each milliwatt of power absorbed. On the other hand, for a material with a much lower thermal conductivity such as SiO_2, the corresponding temperature rise would be much higher, ~190°C/mW of power absorbed. This is important since, as we discuss later, the dc temperature can significantly affect the measurements.

Figure 3(b) shows the dependence of $T_2(0)/T_1(0)$ as a function of a/μ. As can be seen, $T_2(0) \leq T_1(0)$ for all modulation frequencies, saturating at the lower frequencies $a/\mu < 1$ and approaching 1-D behavior in the limit of high-frequency $a/\mu > 1$.

It is important to note that Eq. (2b) is a Gaussian-weighted Hankel transform[27] of the solution to the corresponding 1-D heat conduction problem, where the Gaussian factor $\exp(-q^2a^2/4)$ is the Hankel transform of the incident beam profile $\exp(-r^2/a^2)$, and that Eq. (2a) is the zero frequency, $\omega \to 0$, limit of Eq. (2b). This is, in general, the method for solving any planar problem having an axially symmetric source term and is, in fact, how we extended the 1-D O-R model to three dimensions. Rather than go into mathematical detail, it is perhaps more illuminating to illustrate with examples.

For a layer of thickness d on an infinite half-space we have for the ac surface temperature

$$T_2(r) = \frac{a^2}{2}\left|\int qdq\, \exp(-q^2a^2/4)J_0(qr)\tilde{T}_2(q)\right|, \tag{4a}$$

where $\tilde{T}_2(q)$ is the 1-D solution in the O-R model

$$\tilde{T}_2(q) = \frac{Q_0}{Z_1}\left[\frac{Z_1 + Z_2\tanh(q_{1z}d)}{Z_2 + Z_1\tanh(q_{1z}d)}\right]. \tag{4b}$$

In this latter expression, q_{1z} and q_{2z} are complex thermal-wave vector components in the z direction in the layer and substrate, respectively, defined in terms of thermal diffusion lengths,

$$q_{jz} = \sqrt{q^2\mu_j^2 - 2i}/\mu_j,$$

and Z_j are thermal-wave impedances (similarly defined in the O-R model), $Z_j = \kappa_j q_{jz}$ for $j = 1,2$. Also, Q_0 is the energy flux $Q_0 = P_0/\pi a^2$. In the dc limit $\omega \to 0$ we have

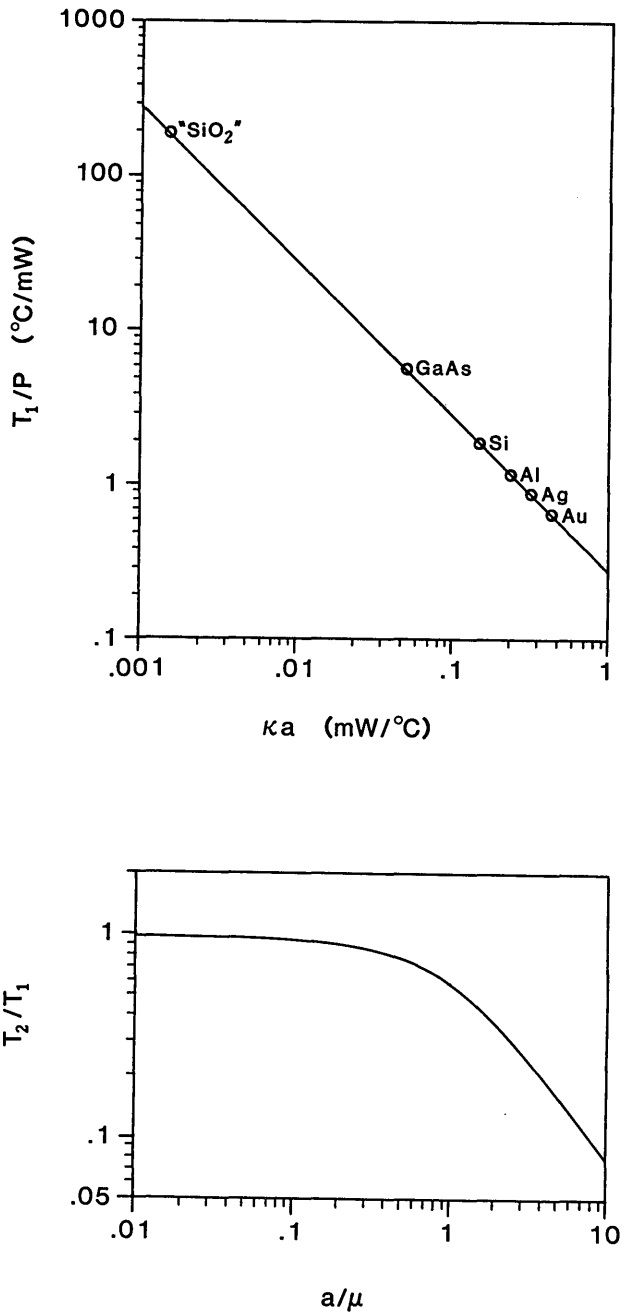

Fig. 3. Surface temperatures of the center of the heating beam (a) per milliwatt of power absorbed for a variety of materials at zero modulation frequency and (b) ac temperature normalized to the dc temperature as a function of the ratio of beam radius to the thermal diffusion length.

$Z = q\kappa_j$. Consequently, as one can see from Fig. 3(b), at low frequencies, where $a/\mu < 1$,

$$T_2(r) \simeq T_1(r) = \frac{a^2}{2}\int qdq\, \exp(-q^2a^2/4)J_0(qr)\tilde{T}_1(q), \quad (5a)$$

where

$$\tilde{T}_1(q) = \frac{Q_0}{q\kappa_1}\left[\frac{\kappa_1 + \kappa_2\tanh(qd)}{\kappa_2 + \kappa_1\tanh(qd)}\right]. \quad (5b)$$

Although not obvious at this point, the maximum sensitivity of the thermal wave to film thickness variation occurs in general for $d \ll \mu$ and, at low frequencies, for $d < a$.

The explicit dependence on thickness for thin films is easily found in the limit of zero frequency from Eqs. (5a) and (b) to be

$$T_2(r) \simeq T_1(r) = \frac{P_0}{2\sqrt{\pi}\kappa_2 a}\left[\exp(-r^2/2a^2)I_0(r^2/2a^2) + \frac{2}{\sqrt{\pi}}\left(\frac{d}{a}\right) \times \exp(-r^2/a^2)\left(\frac{\kappa_2}{\kappa_1} - \frac{\kappa_1}{\kappa_2}\right)\right], \quad (6)$$

where $I_0(x) = J_0(ix)$ is the modified Bessel function of order zero. For points near the center of the heating beam $r \ll a$ we have

$$T_2(r) \simeq T_1(r) = \frac{P_0}{2\sqrt{\pi}\kappa_2 a}\left[1 + \frac{2}{\sqrt{\pi}}\left(\frac{d}{a}\right)\left(\frac{\kappa_2}{\kappa_1} - \frac{\kappa_1}{\kappa_2}\right) - 0(r^2/a^2)\right] \quad (7a)$$

and, in the limit of $r \gg a$,

$$T_2(r) \simeq T_1(r) = \frac{P_0}{2\pi\kappa_2 r}\left[1 + 2\left(\frac{d}{a}\right)\left(\frac{r}{a}\right)\exp(-r^2/a^2)\left(\frac{\kappa_2}{\kappa_1} - \frac{\kappa_1}{\kappa_2}\right)\right], \quad (7b)$$

indicating that the sensitivity to layer thickness will fall off quite rapidly as one moves away from the center of the beam. In a measurement dependent only on thermal-wave parameters this would more than likely be observed, but for measurements such as we are reporting here, in which thermoelastic and optical effects are also significant, one can expect some differences to occur.

B. Surface Deformations

In our experiments we do not measure the local surface temperatures directly but, rather, the local surface deformations which depend on average temperature. An infinitesimal probe beam incident normal to the surface at distance r from the center of the thermally induced surface deformation will undergo a periodic deflection $\delta(r)$, where

$$\delta(r) = \delta_1(r) + \delta_2(r)\cos(\omega t + \psi). \quad (8)$$

The deflection is related to the surface displacement $u(r)$ by

$$\delta(r) = 2\frac{du}{dr}, \quad (9)$$

and $u(r)$ is given by

$$u(r) = \frac{a^2}{2}\int qdq\, \exp(-q^2a^2/4)J_0(qr)\tilde{u}(q), \quad (10)$$

where $\tilde{u}(q)$ is the solution to the corresponding 1-D thermoelastic problem. From Eqs. (9) and (10) we then have

$$\delta_1(r) = -a^2\int q^2dq\, \exp(-q^2a^2/4)J_1(qr)\tilde{u}_1(q), \quad (11a)$$

$$\delta_2(r) = -a^2\int q^2dq\, \exp(-q^2a^2/4)J_1(qr)\tilde{u}_2(q), \quad (11b)$$

where $J_1(qr)$ is the Bessel function of order 1. As with the temperatures $T_1(r)$ and $T_2(r)$, the thermoelastic deflections $\delta_1(r)$ and $\delta_2(r)$ obey the relationship $\delta_2(r) \to \delta_1(r)$ as $\omega \to 0$.

Applying the O-R model to the problem of a single layer on a half-space results in a complicated expression for the ac component, which, in the limit of a thin film, simplifies to

$$\tilde{u}_2(q) = \frac{-\gamma_2 Q_0}{(q + q_{2z})Z_2}\left\{1 + q_{1z}d\left[\left(\frac{q + q_{2z}}{q_{1z}}\right)\left(\frac{\gamma_1 - \gamma_2}{\gamma_2}\right) - \left(\frac{q_{2z}}{q_{1z}}\right)\left(\frac{q_{1z}Z_1 - q_{2z}Z_2}{q_{2z}Z_2}\right)\right]\right\}, \quad (12)$$

where γ_j are the thermoelastic coupling factors, $\gamma_j = \alpha_j(1 + \nu_j)/(1 - \nu_j)$, α_j the thermal expansion coefficients, and ν_j the Poisson's ratios for $j = 1,2$.

Taking the limit $\omega \to 0$ yields for the dc limit,

$$\tilde{u}_1(q) = \frac{-\gamma_2 Q_0}{2q^2\kappa_2}\left\{1 + qd\left[2\left(\frac{\gamma_1 - \gamma_2}{\gamma_2}\right) - \left(\frac{\kappa_1 - \kappa_2}{\kappa_2}\right)\right]\right\}. \quad (13)$$

Since the product $q_{jz}Z_j$ becomes independent of κ_j in the high-frequency limit $a/\mu \gg 1$, we see the possibility for markedly different behavior in passing from high frequencies to the dc limit.

Performing the required integration for the dc terms in Eq. (11), we find for the thin film deflection at low ω $(a/\mu < 1)$,

$$\delta_2(r) \simeq \delta_1(r) = \frac{\gamma_2 P_0}{2\pi\kappa_2 a}\left\{\frac{a}{r}\left[1 - \exp(-r^2/a^2)\right] + \sqrt{\pi}\left(\frac{d}{a}\right)\left(\frac{r}{a}\right)\left[2\left(\frac{\gamma_1 - \gamma_2}{\gamma_2}\right) - \left(\frac{\kappa_1 - \kappa_2}{\kappa_2}\right)\right] \times \exp(-r^2/2a^2)[I_0(r^2/2a^2) - I_1(r^2/2a^2)]\right\}, \quad (14)$$

which for small r, $r < a$ gives

$$\delta_2(r) \simeq \delta_1(r) = \frac{\gamma_2 P_0}{2\pi\kappa_2 a}\left(\frac{r}{a}\right)\left\{1 + \sqrt{\pi}\left(\frac{d}{a}\right)\left[2\left(\frac{\gamma_1 - \gamma_2}{\gamma_2}\right) - \left(\frac{\kappa_1 - \kappa_2}{\kappa_2}\right)\right]\right\} \quad (15a)$$

and for $r > a$,

$$\delta_2(r) \simeq \delta_1(r) = \frac{\gamma_2 P_0}{2\pi\kappa_2 r}\left\{1 + \left(\frac{d}{r}\right)\left[2\left(\frac{\gamma_1 - \gamma_2}{\gamma_2}\right) - \left(\frac{\kappa_1 - \kappa_2}{\kappa_2}\right)\right]\right\}. \quad (15b)$$

Although there is some loss of sensitivity to thickness variation with increasing r, it is not as severe as in the surface temperature. Also, at finite frequencies there can be a gain in sensitivity depending on the parameters involved.

C. Thermal Lens Effects

Now the probe beam, in addition to being deflected by the local surface deformation, will also be deflected as depicted in Fig. 2 by the thermal-wave-induced index of refraction gradient in the air above the sample surface (and, for that matter, in any transparent material whose index of refraction varies with temperature). Considering again an infinitesimal probe beam at normal incidence, we have for the deflection occurring in the air above an opaque sample

$$\xi(r) = \xi_1(r) + \xi_2(r)\cos(\omega t + \chi). \tag{16}$$

This can be expressed in terms of the surface temperatures by integrating along the beam path (z direction) the radial derivative of the temperature, that is,

$$\xi(r) = -2\varepsilon \int dz \frac{dT}{dr}, \tag{17}$$

where ε is the normalized temperature derivative of the index of refraction $\varepsilon = -1/n\, dn/dT$, and the factor of 2 accounts for the deflection taking place along both the incident and reflected paths. Again employing the O-R model for thermal waves in layered media we have

$$\xi_1(r) = \varepsilon a^2 \int q dq \exp(-q^2a^2/4) J_1(qr) \tilde{T}_1(q), \tag{18a}$$

$$\xi_2(r) = \varepsilon a^2 \int q^2 dq \exp(-q^2a^2/4) J_1(qr) \frac{\tilde{T}_2(q)}{q_{0z}}, \tag{18b}$$

where q_{0z} is the thermal wave vector in air, and $\tilde{T}_1$ and $\tilde{T}_2$ are given, respectively, by Eqs. (5b) and (4b). For a thin film we have the results at low frequencies ($a/\mu < 1$),

$$\xi_2(r) \simeq \xi_1(r) = \frac{\varepsilon P_0}{\pi \kappa_2 a}\left(\frac{r}{a}\right)\left[1 + \sqrt{\pi}\left(\frac{d}{a}\right)\left(\frac{\kappa_2}{\kappa_1} - \frac{\kappa_1}{\kappa_2}\right)\right], \tag{19a}$$

when $r \ll a$, and when $r \gg a$,

$$\xi_2(r) \simeq \xi_1(r) = \frac{\varepsilon P_0}{\pi \kappa_2 r}\left[1 + \left(\frac{d}{r}\right)\left(\frac{\kappa_2}{\kappa_1} - \frac{\kappa_1}{\kappa_2}\right)\right]. \tag{19b}$$

D. Other Effects

The theory presented above, while by no means complete, does contain the essential features of thermal-wave physics that enable us to better understand our experimental results. The most important effects that remain are those associated with having a finite probe beam, finite absorption length, and nonlinear effects due to significant temperature dependencies in some of the material parameters. The complexities introduced by the full elastic Green's function are fortunately not present here, since measurements in the immediate vicinity of the thermal wave are completely dominated by temperature and the accompanying scalar thermal expansion response.

The effects of using a finite probe beam are included by introducing an additional Gaussian factor, $\exp(-q^2b^2/4)$, in the Hankel transform, where b is the radius of the probe beam. In the results presented below, $b = 0.75a$ as determined experimentally.

We include the effects of finite optical absorption in the sample by the linear superposition of temperature solutions corresponding to a distribution of subsurface heat sources. In almost all cases of practical significance, the source distribution is well approximated by an exponential $\beta P_0 \exp(-\beta z)$, where β^{-1} is the absorption length, and P_0 is the total power absorbed. For a 488-nm heating beam on Al, $\beta \simeq 10^6\ \mathrm{cm}^{-1}$, which, at the modulation frequencies used in our measurements, means that essentially all the energy is absorbed at the surface. On the other hand, in Si, $\beta \simeq 10^4\ \mathrm{cm}^{-1}$, corresponding to an absorption length approximately half of the thermal diffusion length at the highest frequency used, 10 MHz. In all our measurements (for Si and SiO_2-on-Si) the finite absorption reduces the magnitude of the thermal wave but does not significantly alter its dependence on frequency or thickness.

Nonlinear effects and their inclusion in the analysis are described in Sec. III, and a full discussion will be given in another paper.

Before presenting our results there is one important point that needs to be made. In the O-R model it was shown that the thermoelastic response at the back surface of a sample being heated at a mechanically constrained front surface is independent of variations in thermal conductivity. Basically this resulted from the response being proportional to the average temperature in the heated region. By the same token, this same lack of dependence on thermal conductivity occurs here for the front surface displacements in the heated region at high frequencies since it, too, becomes a simple 1-D average of temperature. What is important to note is that such a varying dependence on thermal conductivity in going from low (3-D) to high frequency (1-D) is characteristic of all thermal-wave effects and is one of the more fundamental reasons that truly quantitative measurements of thermal features are possible.

III. Results

Of considerable interest is establishing the relative significance of the thermoelastic and thermal lens effects on the deflection of the probe beam. For this we consider the deflections from an opaque homogeneous substrate with no layers as depicted in Fig. 2. Setting $d = 0$ in Eqs. (10)–(14) yields for the thermoelastic deflections

$$\delta_1(r) = \frac{\gamma T_1(0)}{\sqrt{\pi}}\left(\frac{a}{r}\right)[1 - \exp(-r^2/a^2)], \tag{20a}$$

$$\frac{\delta_2(r)}{\delta_1(r)} = \frac{2(r/\mu)}{1 - \exp(-r^2/a^2)} \times \left| \int x^2 dx \frac{J_1(rx/\mu)\exp(-a^2x^2/4\mu^2)}{\sqrt{x^2 - 2i}(x + \sqrt{x^2 - 2i})} \right|. \tag{20b}$$

At all frequencies ω, $\delta_2(r) \leq \delta_1(r)$ and $\delta_2(r) \to \delta_1(r)$ as $\omega \to 0$. In our experiments only the ac component $\delta_2(r)$ is measured. When $a/\mu < 2$, the theory predicts that the maximum $\delta_2(r)$ occurs at $r = 1.1a$ in agreement with our experimental results. The dependence of $\delta_1(r)$ and $\delta_2(r)$ on the thermoelastic coupling factor γ can be most important in performing depth profiling of layered materials, since γ can vary significantly for different materials. For example, $\gamma = 49 \times 10^{-6}/°\mathrm{C}$ in Al and only $3.7 \times 10^{-6}/°\mathrm{C}$ in Si. Thus, even though the surface

temperatures in these two materials would be comparable under the same heating conditions, the beam deflection from an Al surface would be approximately ten times greater than from a Si surface. Using a more complete model that accounts for optical reflectivities, finite absorption depths, and finite probe beam diameters, we have calculated the relative laser beam deflections from Al and Si as a function of modulation frequency. The results shown by the dashed curves in Fig. 4 are found to be in excellent agreement with the experimental results plotted as open circles on the same figure.

The thermal lens effects occur in the air above the sample surface and within any layer of the sample that is not optically opaque. Even though these thermal lenses have only micron-sized dimensions at the high modulation frequencies employed, their refractive power is still considerable since the normalized refractive-index gradient $n^{-1}(dn/dx) = -\varepsilon(dT/dx)$ across the lens is now quite high, ε being of the same order as the thermal expansion coefficient of a solid. Also, even though the probe laser beam is incident normal to the sample surface, it strikes the thermal lens off-axis and thus undergoes refraction in both incident and reflected directions. Consequently, the theory predicts and we find experimentally that the thermal lens effect can be appreciable for some materials such as Si.[28]

From Eqs. (18a) and (b) we obtain for the thermal lens deflection of an infinitesimal probe beam at a distance r from the center of the heated region

$$\xi_1(r) = \frac{2\varepsilon}{\gamma}\delta_1(r), \tag{21a}$$

$$\frac{\xi_2(r)}{\xi_1(r)} = \frac{r/\mu}{1-\exp(-r^2/a^2)} \left| \int x^2 dx \frac{J_1(rx/\mu)\exp(-a^2x^2/4\mu^2)}{x^2-2i} \right| . \tag{21b}$$

Note that, while this result Eq. (21b) is similar to Eq. (20b) for the corresponding thermoelastic effect, we would expect because of the different integrands a slightly different dependence on frequency. Equation (21b) will approach 1-D behavior more rapidly than Eq. (20b).

For air at 1 atm and 0°C, $\varepsilon = 1.1 \times 10^{-6}$/°C,[29] and thus $\xi_1(r)/\delta_1(r)$ for Si is ~0.6 and for Al is ~0.05. However, nonlinear effects due to higher temperatures (to be discussed later) will tend to reduce these ratios. Figure 4 presents comparisons with experiments for a complete calculation (that includes nonlinearities) under vacuum, where there is no thermal lens effect (dashed curves), and in air, where there is a thermal lens effect (solid curves). The agreement between theory and experiment is excellent. Note that the somewhat stronger dependence on frequency predicted for the thermal lens effect is observed experimentally in that its contribution to the total measurement decreases with increasing frequency.

In these thermal-wave experiments dc and ac temperature excursions can range from 30°C to several hundred degrees depending on the sample's thermal characteristics. With such temperature excursions, the

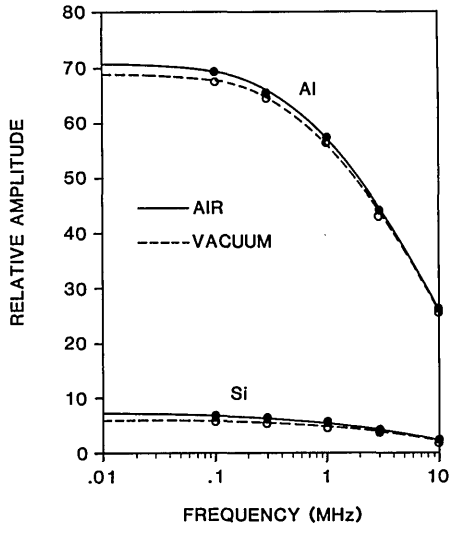

Fig. 4. Relative amplitude of laser beam deflection signal as a function of thermal-wave (modulation) frequency for Al and Si under air (with thermal lens) and vacuum (no thermal lens) conditions. Experimental data are plotted as open (vacuum) and closed (air) circles and theoretical results as dashed (vacuum) and solid (air) curves.

dependence on temperature of the various thermal, optical, and elastic parameters has to be considered as well. In general, the most critical parameters appear to be the refractive index and the thermal conductivity. The index of refraction of air is given by[29]

$$n = 1 + \frac{n_0 - 1}{1 + \alpha_v T}P, \tag{22}$$

where $n_0 = 1.003$ is the index of refraction of air at 0°C, T is the temperature above 0°C, $\alpha_v = 3.66 \times 10^{-3}$/°C is the volume thermal expansion coefficient, and P is the normalized pressure of the air. Thus for temperature excursions in air of 10–100°C, ε will decrease by 30–50%. In addition, for most solids the temperature dependence of the thermal conductivity at our operating temperatures is given by[30]

$$\kappa(T) = \frac{\kappa_0}{1 + \beta_\kappa T}, \tag{23}$$

where κ_0 is the thermal conductivity at $T = 0$°C, T is the temperature above 0°C and, β_κ is a temperature coefficient. Temperature excursions of 50–100°C in Si, where $\beta_\kappa = 7.1 \times 10^{-3}$/°C,[30] thus decreasing κ by 30–60%. These temperature effects on ε and κ introduce appreciable nonlinearities in the model that cannot be neglected.

Optical effects will, of course, play an important role in these experiments as well. For example, in Si we have to take into account the optical absorption length (~1 μm) for the 488-nm Ar^+ ion laser light. Optical reflectivities must also be included. In addition, when dealing with optically transparent films such as SiO_2, optical interference effects within the film have to be considered as well. Figure 5 schematically depicts the situation encountered for an SiO_2 film on Si. Here we see the thermoelastic deformations of both the Si–SiO_2

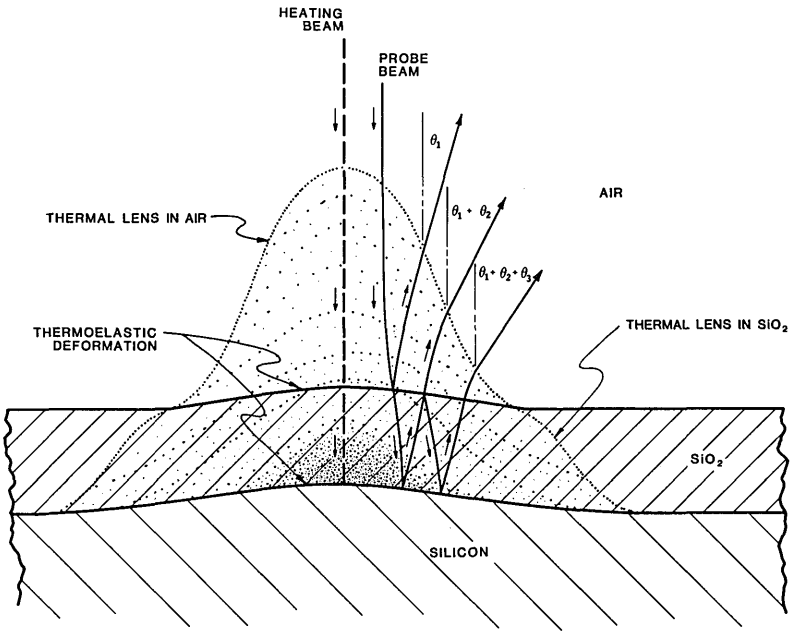

Fig. 5. Schematic depiction of physical processes affecting the laser probe beam for SiO_2 on Si, including thermoelastic deformations of Si–SiO_2 and SiO_2–air interfaces, thermal lenses of opposite sign in air and SiO_2, and optical interference effects in the SiO_2 film.

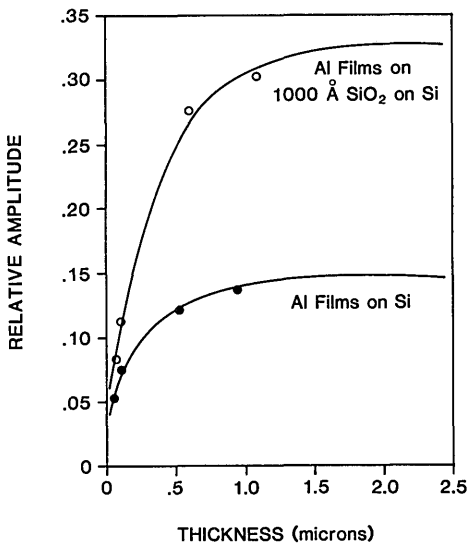

Fig. 6. Relative amplitude at 1 MHz of laser beam deflection signal as a function of Al film thickness for a series of Al-on-Si and Al-on-SiO_2-on-Si films. Circles are experimental data, and curves are from the extended Opsal-Rosencwaig model.

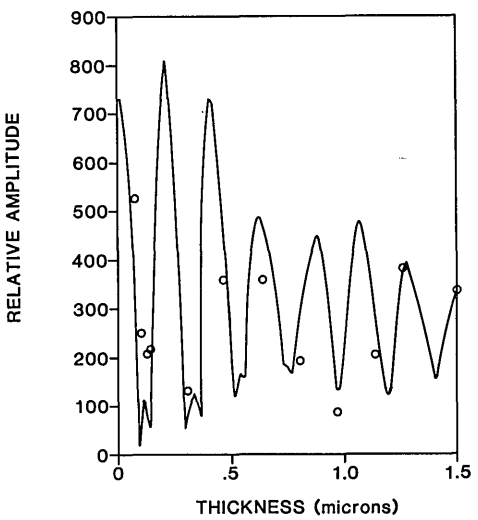

Fig. 7. Relative amplitude at 1 MHz of laser beam deflection signal as a function of SiO_2 film thickness for a series of SiO_2-on-Si films. Circles are experimental data, and curves are from the extended Opsal-Rosencwaig model.

and the SiO_2–air surfaces, the thermal lenses in both the SiO_2 and the air, and the optical interference effects on the probe beam in the SiO_2 film. Note that the thermal lenses have opposite signs in air and SiO_2 because of the opposite signs of their respective ε.

When all the thermal lens optical and nonlinear effects are properly included in the 3-D O-R model, we have a quantitative tool for measuring the thickness of thin films. This is illustrated in Fig. 6, where we show theoretical curves and data obtained for single films of Al on Si and for double films of Al and SiO_2 on Si. We have used the magnitude of the thermal-wave signal rather than the phase in these measurements, since the magnitude has a greater dynamic range and can be measured more precisely. The data in Fig. 6 are in excellent agreement with the theory both for the single and double films. The precision of the readings obtained with a 1-sec averaging time and 1-MHz modulation frequency translates to a thickness sensitivity of $\pm 2\%$ over the thickness range of 500–25,000 Å for these films.

In Fig. 7 we show the theoretical curves and the data for a series of transparent SiO_2 films on Si. Although SiO_2 on Si is only a single film problem, the theory in this case must include thermoelastic deformations at both Si–SiO_2 and SiO_2–air interfaces, thermal lens effects in both the SiO_2 and the air, and optical interference effects in the SiO_2 (see Fig. 5). The fit between theory and experiment is, with all this complexity, quite good, indicating that transparent as well as opaque films

can be measured with this thermal-wave technique. The thickness sensitivity for SiO_2 films on Si appears to be ±2% over the 500–15,000 Å range.

IV. Conclusions

We have developed a method for measuring the thickness of opaque and transparent thin films by combining a new laser beam deflection technique with a 3-D model of thermal-wave propagation in layered media. The experimental part of our technique is unique in that both the heating and probe laser beams are highly focused, directed normal to the sample surface, and offset by a small distance from each other. With this apparatus we measure both thermally induced surface deformations and thermal lens effects at modulation frequencies up to and including 10 MHz. As we have shown, however, the surface deformations are more significant even for materials with relatively low thermal expansion coefficients such as Si, and at the highest modulation frequencies (10 MHz) the surface deformations completely dominate the measurements.

The theory comprising the other half of our methods is an extension to three dimensions of the Opsal-Rosencwaig model of thermal-wave propagation and response in multilayered systems. In this paper we illustrated with examples the essential elements of the extended theory showing results for limiting cases that closely approximate the conditions for which our technique is most sensitive to thickness variations. In addition to explaining the measurements, the theory is also embodied in a formalism that allows for the systematic treatment of very complex structures including layered media, in which the heating beam energy is absorbed beneath the surface, and transparent layers, in which optical interference effects on the probe beam are modulated by the thermal waves. We have also found that nonlinear effects due to temperature dependencies in material parameters, particualrly thermal conductivity and index of refraction, are significant and must be included.

We believe that the combination of our experimental system and theoretical model provides for the first time a truly quantitative (i.e., accurate) method for efficiently measuring both opaque and transparent thin film thicknesses in a nondestructive and noncontact manner.

References

1. A. Rosencwaig, *Photoacoustics and Photoacoustic Spectroscopy* (Wiley, New York, 1980).
2. R. L. Swofford, M. E. Long and A. C. Albrecht, J. Chem. Phys. **65,** 179 (1979).
3. P. Korpiun and R. Tilgner, J. Appl. Phys. **51,** 6115 (1980).
4. A. Rosencwaig, Science **218,** 223 (1982).
5. Y. H. Pao, Ed., *Optoacoustic Spectroscopy and Detection* (Academic, New York, 1977).
6. M. Luukkala, in *Scanned Image Microscopy*, E. A. Ash, Ed. (Academic, London, 1980), p. 273.
7. G. Busse, in Ref. 6, p. 341.
8. P.-E. Nordal and S. O. Kanstad, in Ref. 6, p. 331.
9. D. Fournier and A. C. Boccara, in Ref. 6, p. 347.
10. W. B. Jackson, N. M. Amer, A. C. Boccara, and D. Fournier, Appl. Opt. **20,** 1333 (1981).
11. J. C. Murphy and L. C. Aamodt, Appl. Phys. Lett. **38,** 196 (1981).
12. S. Ameri, E. A. Ash, V. Neuman, and C. R. Petts, Electron. Lett. **17,** 337 (1981).
13. M. A. Olmstead, S. E. Kohn, and N. M. Amer, Bull. Am. Phys. Soc. **27,** 227 (1982).
14. M. A. Olmstead, N. M. Amer, S. Kohn, D. Fournier, and A. C. Boccara, Appl. Phys. A, accepted for publication.
15. M. A. Olmstead and N. M. Amer, J. Vac. Sci. Technol., accepted for publication.
16. A. Rosencwaig, J. Opsal and D. L. Willenburg, *1983 Photoacoustics Conference.*
17. A. Hordvick and H. Schlossberg, Appl. Opt. **16,** 101 (1977).
18. C. K. N. Patel and A. C. Tam, Rev. Mod. Phys. **53,** 517 (1981).
19. G. S. Cargill, Phys. Today **34,** 27 (Oct. 1981).
20. A. Rosencwaig, Solid State Technol. **25,** 91 (1982).
21. G. Busse and A. Rosencwaig, Appl. Phys. Lett. **36,** 815 (1980).
22. R. M. de la Rue, R. F. Humphreys, I. M. Mason, and E. A. Ash, Proc. Inst. Electr. Eng. **119,** 117 (1972).
23. R. L. Whitman and A. Korpel, Appl. Opt. **8,** 1567 (1969).
24. J. Opsal and A. Rosencwaig, J. Appl. Phys. **53,** 4240 (1982).
25. L. C. Aamodt and J. C. Murphy, J. Appl. Phys. **52,** 4903 (1981).
26. F. A. McDonald, J. Appl. Phys. **52,** 381 (1981).
27. P. Morse and H. J. Feshbach, *Methods of Theoretical Physics, Part I* (McGraw-Hill, New York, 1953), p. 942.
28. Thermal lens effects in the air appear to play a much smaller role in the laser probe method described in Refs. 13–15 because the probe beam in this method is not normal to the sample surface, and thus there is considerable cancellation of the thermal lens deflection as the probe beam traverses different regions of the thermal lens.
29. D. E. Gray, Ed., *American Institute of Physics Handbook,* (McGraw-Hill, New York, 1972), Table 6e-5.
30. D. L. Kwong and D. M. Kim, J. Appl. Phys. **54,** 366 (1983).